7-9-2022

Multiplexed Monitoring of Neurochemicals via Electrografting-Enabled Site-Selective Functionalization of Aptamers on Field-Effect Transistors

Zan Gao

Guangfu Wu

Yang Song

Huijie Li

Yuxuan Zhang

See next page for additional authors

Authors

Zan Gao, Guangfu Wu, Yang Song, Huijie Li, Yuxuan Zhang, Michael J. Schneider, Yingqi Qiang, Jackson Kaszas, Zhengyan Weng, He Sun, Bryan D. Huey, Rebecca Lai, and Yi Zhang

Multiplexed Monitoring of Neurochemicals via Electrografting-Enabled Site-Selective Functionalization of Aptamers on Field-Effect Transistors

Zan Gao,[||] Guangfu Wu,[||] Yang Song,[||] Huijie Li, Yuxuan Zhang, Michael J. Schneider, Yingqi Qiang, Jackson Kaszas, Zhengyan Weng, He Sun, Bryan D. Huey, Rebecca Y. Lai, and Yi Zhang*

ACCESS | 📊 Metrics & More | 📖 Article Recommendations | 🆂�🅸 Supporting Information

ABSTRACT: Neurochemical corelease has received much attention in understanding brain activity and cognition. Despite many attempts, the multiplexed monitoring of coreleased neurochemicals with spatiotemporal precision and minimal crosstalk using existing methods remains challenging. Here, we report a soft neural probe for multiplexed neurochemical monitoring via the electrografting-assisted site-selective functionalization of aptamers on graphene field-effect transistors (G-FETs). The neural probes possess excellent flexibility, ultralight mass (28 mg), and a nearly cellular-scale dimension of 50 μm × 50 μm for each G-FET. As a demonstration, we show that G-FETs with electrochemically grafted molecular linkers (−COOH or −NH$_2$) and specific aptamers can be used to monitor serotonin and dopamine with high sensitivity (limit of detection: 10 pM) and selectivity (dopamine sensor >22-fold over norepinephrine; serotonin sensor >17-fold over dopamine). In addition, we demonstrate the feasibility of the simultaneous monitoring of dopamine and serotonin in a single neural probe with minimal crosstalk and interferences in phosphate-buffered saline, artificial cerebrospinal fluid, and harvested mouse brain tissues. The stability studies show that multiplexed neural probes maintain the capability for simultaneously monitoring dopamine and serotonin with minimal crosstalk after incubating in rat cerebrospinal fluid for 96 h, although a reduced sensor response at high concentrations is observed. Ex vivo studies in harvested mice brains suggest potential applications in monitoring the evoked release of dopamine and serotonin. The developed multiplexed detection methodology can also be adapted for monitoring other neurochemicals, such as metabolites and neuropeptides, by simply replacing the aptamers functionalized on the G-FETs.
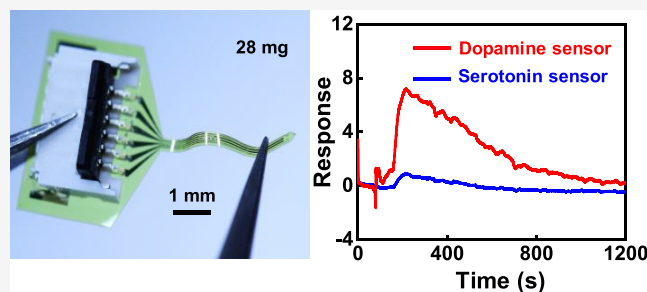
1. INTRODUCTION

Complex behaviors, such as cognition, perception, and action, are conducted through dynamic neural networks of the brain, which are subject to the transmission of neurochemicals.[1,2] More than 200 neurochemicals have been identified in the brain, including monoamines (dopamine (DA), serotonin), peptides, amino acids, lipids, and other small molecules (e.g., acetylcholine).[3,4] The abnormal level of certain types of neurochemicals is related to various neuropsychiatric and neurological disorders, such as Parkinson's disease,[5−10] schizophrenia,[11] and Alzheimer's disease.[12] Many studies have demonstrated the corelease of multiple neurochemicals from neurons.[13−15] For example, increasing evidence has shown that subpopulations of ventral tegmental area (VTA) neurons are capable of releasing glutamate and γ-aminobutyric acid (GABA), or DA and glutamate, simultaneously.[16,17] These diverse signaling mechanisms are directly related to various behaviors and disorders.[18,19] However, our understanding of these multiple neurochemical-involved neurotransmission mechanisms is very limited. This is in part because current measurement technologies have limited spatial/temporal precision and molecular specificity for multiplexed neurochemical identification and detection.

In past decades, with the advances in neuroscience and micro-/nanofabrication, groundbreaking sensors have been developed to target specific brain regions at different scales.[20−22] The main techniques for neurotransmitter monitoring include the following several types: (1) nuclear medicine tomographic imaging, such as positron emission tomography (PET);[23] (2) optical sensing techniques, such as surface-enhanced Raman spectroscopy (SERS),[24,25] fluorescence,[26,27] chemiluminescence,[28] optical fiber biosensing[29] and colorimetry;[30] (3) electrochemical methods,[31−33] like fast-scan cyclic voltammetry (FSCV)[34−36] and amperometry;[37] (4)
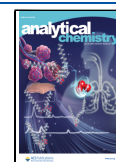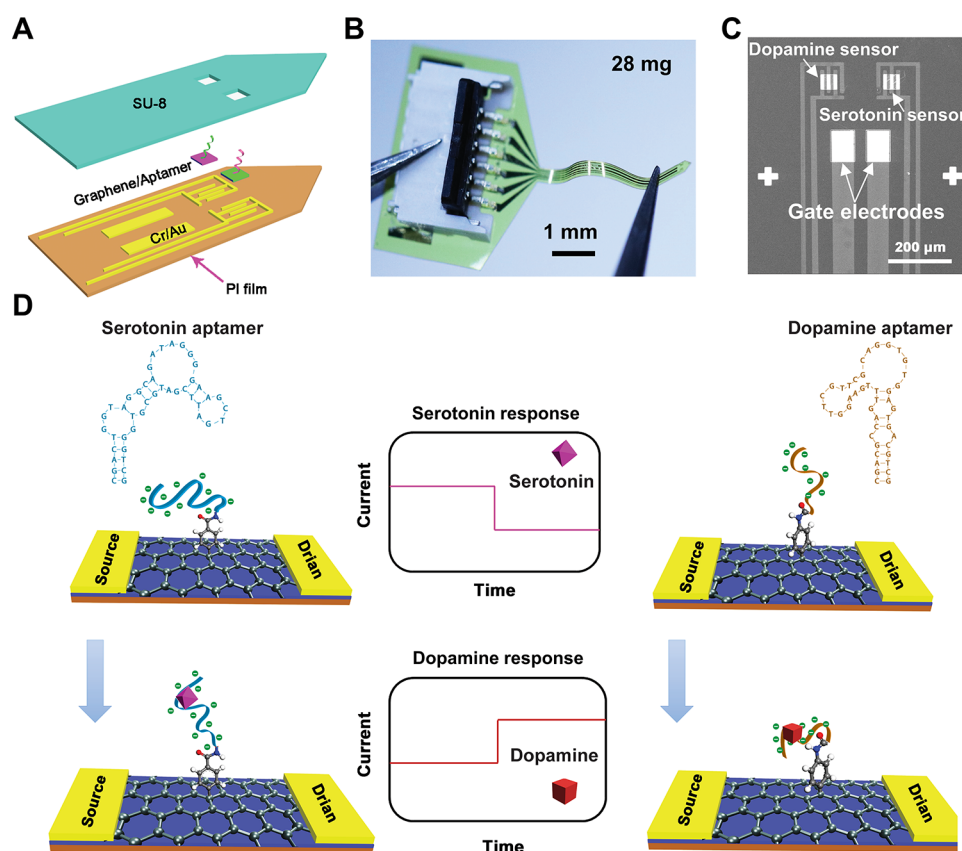
Figure 1. Design, fabrication, and working principle of G-FETs for multiplexed neurochemical monitoring. (A) Schematic illustration and (B) optical images of the G-FETs probe fabricated on (left) 7.6 μm PI (28 mg) for multiplexed neurochemical sensing. (C) SEM image of a representative soft neural probe that consists of two G-FETs, with each G-FET at a nearly cellular-scale dimension (50 μm × 50 μm). (D) Working principles of G-FETs for multiplexed neurochemical monitoring. The graphene surfaces of the two side-by-side G-FETs are selectively functionalized with −COOH and −NH$_2$ groups through electrochemical grafting methods. The electrografted −COOH and −NH$_2$ groups serve as linkers to functionalize two aptamers with different functional groups (−NH$_2$ and −COOH) through EDC/NHS reactions. When dopamine or serotonin binds with the target-specific aptamer, it will cause the conformational change of the functionalized aptamers on the graphene, changing the doping state of the graphene and leading to a measurable source−drain current change of the G-FETs.

mass spectrometry;[25,38,39] and (5) microdialysis sampling (typically coupled with mass spectrometry analysis).[40−44] While each of these techniques has its pros and cons,[4,45,46] it is still a challenge to build a system that can effectively capture the dynamics of neurotransmitter release with a high temporal resolution, cellular scale spatial resolution, superior sensitivity, and selectivity, not to mention empowering the tools with multiplexed monitoring capabilities. Among these methods, FSCV, microdialysis, and genetically encoded fluorescent sensors are three widely used or emerging techniques for neurotransmitter monitoring.[47] Specifically, FSCV possesses better temporal resolution (milliseconds) and sensitivity (nanomolar). Because of that, coupling FSCV or rapid pulse voltammetry with voltammogram analysis (multivariate penalized regression, partial least squares regression, and deep learning) has been used to distinguish voltammograms from multiple neurochemicals, thereby making it possible for multiplexed analysis.[32,48,49] FSCV, however, fails to distinguish some structurally similar neurotransmitters, such as dopamine and norepinephrine.[50−52] Microdialysis suffers from large temporal resolution (typically several minutes) and low spatial resolution because of the semipermeable membrane and large probe size (150−440 μm in diameter).[53,54] Recently, genetically encoded fluorescent sensors have been developed to image the dynamics of neurochemical release in vivo,

including DA and glutamate.[20,55−57] However, the multiplex monitoring with high selectivity and non-overlapping spectra beyond the dual-color imaging of glutamate and DA is challenging.[47] Additionally, the complicated genetic modification process and the requirements of coupling with fiber photometry for neurochemical monitoring limit the practical applications of these genetically encoded sensors.[57]

A previous study reported an aptamer-modified In$_2$O$_3$ field-effect transistor (FET) biosensor for small molecule detection, including serotonin, dopamine, glucose, and sphingosine-1-phosphate under high-ionic strength conditions.[58] However, the large device size and bulky and rigid component materials lead to constrained spatial resolution and potential brain tissue damage, limiting its practical application in in vivo studies. Recently, implantable aptamer-modified field-effect transistors were reported for monitoring serotonin or dopamine in vivo.[59,60] Although these studies represent significant progress for individual neurotransmitter monitoring, like dopamine or serotonin, it is still challenging to achieve simultaneous monitoring of different types of neurochemicals with spatiotemporal precision and molecular specificity.

Here, we report a soft neural probe for multiplexed neurochemical sensing via the electrografting-enabled site-selective functionalization of aptamers on G-FETs. We show that the developed G-FET sensors selectively functionalized
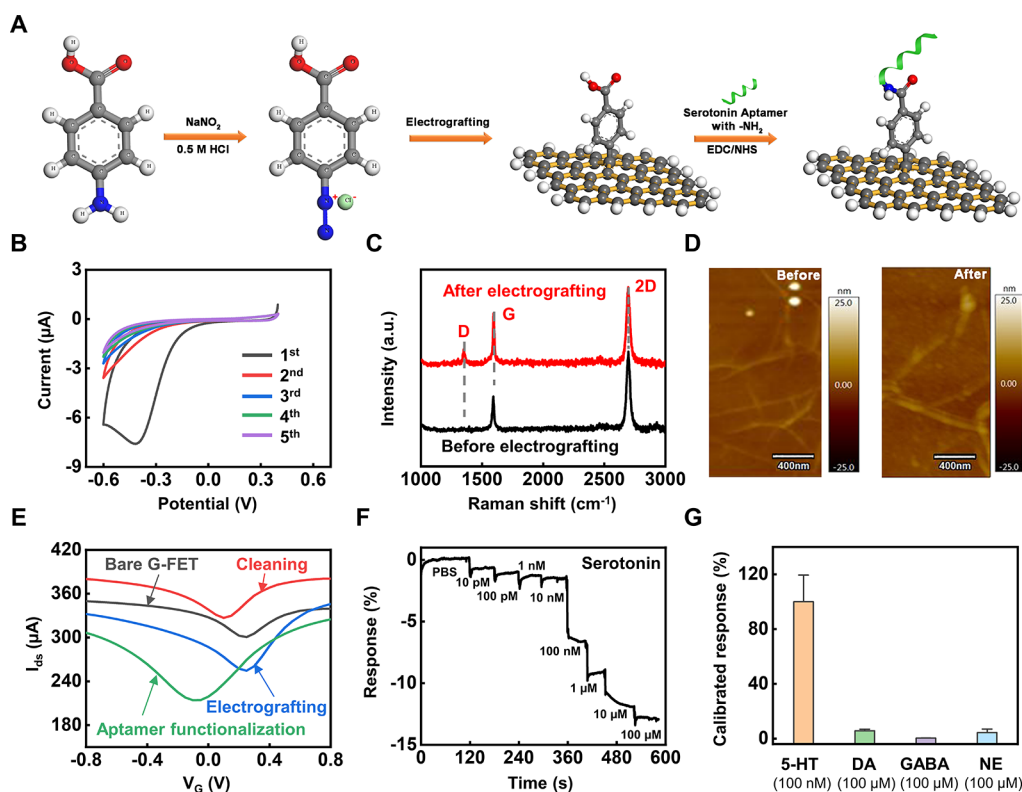
Figure 2. Electrografting of the −COOH group and functionalization of G-FET with serotonin aptamer. (A) Schematic illustration of the electrografting of −COOH group on the graphene surface through diazonium reaction and functionalization of the serotonin aptamer through EDC/NHS reactions. (B) CV curves of the electrografting process to introduce the −COOH group on the graphene surface. (C) Raman spectrum of graphene surface before and after electrografting. (D) AFM images of graphene surface before and after electrografting with the −COOH group. (E) Transfer curves of fabricated G-FETs after different processing steps, including cleaning, electrografting, and aptamer functionalization. V_{ds} = 200 mV. (F) Real-time source−drain current response of the G-FET serotonin sensor upon exposure to 1× PBS solution containing serotonin with different concentrations: 10 pM, 100 pM, 1 nM, 10 nM, 100 nM, 1 μM, 10 μM, and 100 μM. The current response is defined as $\Delta I_{ds}/I_0 \times 100\%$, where ΔI_{ds} and I_0 are the change of the source−drain current in the presence of the target and the initial signal without the target, respectively. V_{ds} = 100 mV; V_G = 0 mV. (G) Selectivity of the serotonin sensor. 5-HT: serotonin; DA: dopamine; NE: norepinephrine; GABA: γ-aminobutyric acid.

with specific aptamers can be used to simultaneously monitor two important neural neurochemicals (serotonin and dopamine) with high sensitivity, selectivity, and minimal interferences. Such a spatially controlled electrochemical functionalization method could potentially empower the G-FET arrays with an increased number of sensing channels for multiplexed neurochemical monitoring, such as dopamine, serotonin, norepinephrine, and neuropeptides, suggesting broad applications in neuroscience research.

2. RESULTS AND DISCUSSION

2.1. Design, Fabrication, and Functionalization of G-FETs for Multiplexed Neurochemical Monitoring. As illustrated in Figure 1A,B, we designed a filament neural probe (∼400 μm wide, ∼8.4 μm thick, and 6.2 mm long), consisting of two side-by-side G-FET sensors that are selectively functionalized with two different types of aptamers and encapsulated with a thin layer of SU-8. The source and drain contact pads (15 nm chromium and 90 nm gold) of G-FET were patterned on a thin-film polyimide (PI, 7.6 μm thick) through photolithography, metal deposition, and lift-off processes (Figure S1A). After that, the chemical vapor deposition (CVD)-grown graphene on copper foil was transferred, patterned, and assembled with the fabricated source and drain electrodes to make the G-FETs (Figure S1B). Finally, the soft G-FET was encapsulated with a lithography-

defined thin layer of SU-8 (∼ 0.8 μm thick). Figure 1B,C shows the optical and SEM images of the fabricated neural probe. The neural probe possesses excellent flexibility and ultralight mass (28 mg) with a nearly cellular-scale dimension of 50 μm × 50 μm for each G-FET, which is much smaller than that of microdialysis probes (150−440 μm in diameter). The ultralow bending stiffness (∼7.9 × 10^{-11} N m^2, a value six orders of magnitude smaller than that of commonly used neural probes, such as a 230 μm outer diameter optical fiber[61]) and lightweight construction allow the implantation of the probe into the deep brain area with reduced tissue damage, inflammation, and motion artifacts.[62−64]

The cleanliness of the graphene surface strongly affects the electronic properties of graphene and the final sensing capabilities of G-FETs. Here, a simple bubble-free electrochemical (EC) treatment was used to rapidly clean the residual polymethyl methacrylate (PMMA) on the graphene surface after the wet transfer process.[65] During the EC treatment, the G-FET was used as the working electrode, Ag/AgCl was used as the reference electrode, and Pt was used as the counter electrode. More specifically, cyclic voltammetry (CV) scans at a scan rate of 0.5 V s^{-1} (−0.7 to 0 V) were performed to remove the residual negatively charged PMMA polymer, de-dope the graphene surface, and recover its intrinsic electrical properties. The cleaned graphene surface was further modified

with a functional group and functionalized with a specific type of aptamer for neurotransmitter monitoring.

The graphene surfaces of the two side-by-side G-FETs were selectively functionalized with −COOH and −NH$_2$ groups through electrochemical grafting methods. The electrografted −COOH and −NH$_2$ groups serve as linkers to anchor two aptamers with different functional groups through the 1-ethyl-3-(3-dimethylaminopropyl) carbodiimide (EDC)/N-hydroxysuccinimide (NHS) reaction (serotonin aptamer: 5′-AmC6-CGA CTG GTA GGC AGA TAG GGG AAG CTG ATT CGA TGC GTG GGT CG-3′; dopamine aptamer: 5′/COOH/CGA CGC CAG TTT GAA GGT TCG TTC GCA GGT GTG GAG TGA CGT CG-3′) for the detection of serotonin and dopamine simultaneously. Typically, the aptamers are attached to the graphene surface through a pyrene-based $\pi{-}\pi$ stacking.[66,67] Although G-FET functionalized with $\pi{-}\pi$ stacking usually has better sensitivity as it does not change the structure of graphene, the weak bonding between aptamer and graphene may make it not ideal for in vivo applications. Different from the widely used noncovalent $\pi{-}\pi$ stacking to anchor aptamer on graphene surface,[67,68] in this study, the EDC/NHS reaction enabled the formation of a covalent bond between the graphene surface and the aptamers,[69,70] which is critical to achieve long-term stability of the designed neural probe in the chronic in vivo study.

G-FETs modified with target-specific recognition components could directly enable biodetection in physiological conditions.[68] However, the shielding effect of the electrical double layer, characterized as Debye screening length,[71] prevents biosensing. Meanwhile, the small target molecules with few or no charges could not trigger enough transconductance change of G-FET, leading to a minimal response. Recent studies showed that aptamers, selected through SELEX,[72] could overcome these limitations for small molecular detection.[58] When small molecular targets, like dopamine and serotonin, bind with the target-specific aptamer, it will cause the conformational change of the anchored aptamers on graphene,[58,73] changing the doping state of graphene and leading to a measurable source−drain current change of the G-FETs (Figure 1D). The change in source−drain current of G-FETs can be correlated with the concentration of dopamine or serotonin (Figure 1D).
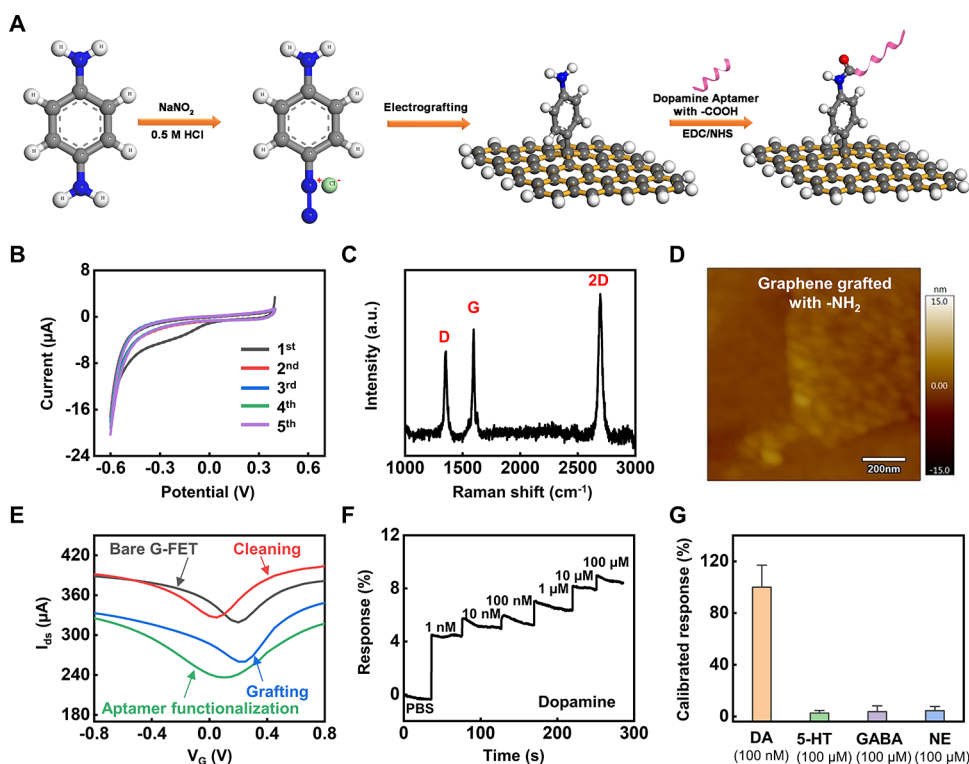
2.2. Electrografting of the −COOH Group and Functionalization of the Serotonin Aptamer on G-FET.
The strategy for developing the serotonin aptamer-functionalized G-FET sensor is illustrated in Figure 2A. Briefly, an aqueous solution of NaNO$_2$ was dropwise added to p-aminobenzoic acid (p-ABA) (0.5 M HCl) to form a homogeneous mixture. The mixed solution was then kept in an ice/water bath to form a diazonium salt (ClN$_2$$^+$-Ph-COOH). The selected G-FET array was then immersed into the above solution and used as a working electrode to link the −Ph-COOH on the graphene surface by applying CV scans from −0.6 to 0.5 V for five cycles (scan rate = 100 mV s^{-1}). During the first cycle, a reduction peak appeared at −0.4 V, which disappeared during the subsequent cycles, and the CV curves gradually became stable after the second scan, indicating the electrochemical reduction of ClN$_2$$^+$-Ph-COOH to form the modified graphene-Ph-COOH surface[74] (Figure 2B). The surface functionalization of graphene with −Ph-COOH can be further proven by the Raman (Figure 2C) and atomic force microscopy (AFM, Figure 2D) tests. The Raman spectra of graphene on G-FET before and after electrochemical grafting

are shown in Figure 2C. There are two prominent peaks for the bare graphene, a single symmetric 2D band at ∼2700 cm^{-1} and a G band at ∼1580 cm^{-1}. The intensity ratio between the 2D band and the G band is around 2.22, which is a typical characteristic of monolayer graphene, indicating that the transferred graphene on G-FET remains in high quality after the transferring process.[75] Furthermore, after the electrografting process, there is a new D band appearing at ∼1350 cm^{-1}, which usually represents the defects and disordered graphite structures.[76] The appearance of the D band indicates the success of the electrochemical grafting reaction, which broke the sp^2 bond of graphene and linked the −Ph-COOH on graphene through the diazonium reaction. The ratio of I_{2D}/I_G, after electrografting of the −COOH group, is 1.47, indicating the binding of the functional −COOH group on the graphene surface. A clear surface morphology change of graphene can be observed from the AFM image after the electrochemical grafting process. As shown in Figure 2D, compared to the pure graphene surface, a much rougher surface with small nanoparticles can be observed from the AFM image of the electrografted graphene surface. The significant surface morphology change could be attributed to the electrografting formation of −Ph-COOH on graphene. The electrografting was further highlighted by the cyclic voltammetric characterization of the graphene surface before and after the electrografting (Figure S2). After electrografting, the anodic current of Fe(CN)$_6$$^{4-}$ to Fe(CN)$_6$$^{3-}$ significantly reduced, suggesting the barriers on the graphene surface to the electron transfer. The grafted −Ph-COOH on graphene serves as a linker to functionalize the serotonin aptamer with an −NH$_2$ group through an EDC/NHS reaction.

Figure 2E shows the transfer curves of the fabricated G-FETs after electrochemical cleaning, electrografting, and aptamer functionalization. Clearly, after the electrochemical cleaning process, there is an upward left shift of the V-shaped transfer curve. The slightly increased current response and left shift of the Dirac point suggested that the electrochemical cleaning increased the conductivity and changed the doping state of the graphene.[66,68] The downward and right shift of the transfer curve after the electrografting of the −COOH group further proves the successful diazonium reaction, which broke the sp^2 bond of graphene and introduced the −Ph-COOH group, leading to the increased resistance and reduced current response. After the serotonin aptamer functionalization with the EDC/NHS reaction, we can see a downward left shift of the transfer curve, mainly due to the non-electrostatic stacking interactions between the aptamer and the graphene or the donor effect.[68]

To quantify the sensing performance of the functionalized G-FET serotonin sensor, the probe was exposed to the target solution with various concentrations to record the source−drain current (I_{ds}). The electrical response is defined as $\Delta I_{ds}/I_0 \times 100\%$, where ΔI_{ds} is the source−drain current change caused by the addition of serotonin and I_0 is the initial signal without the addition of serotonin. During the measurement, the gate voltage V_G was fixed at 0 mV to avoid possible chemical reactions such as water electrolysis, dielectric layer breakdown, and the denaturing of the recognition components. As seen in Figure 2F, the electrical response decreases as the increase of serotonin concentration ranging from 10 pM to 100 μM in phosphate-buffered saline) (1× PBS, pH 7.4), which covers the physiologically relevant serotonin concentration in cerebrospinal fluid (CSF).[45,77] The serotonin sensor achieves a limit of

Figure 3. Electrografting of the −NH$_2$ group and functionalization of G-FET with dopamine aptamers. (A) Schematic illustration of the electrografting of the −NH$_2$ group on the graphene surface through the diazonium reaction and the functionalization of the dopamine aptamer through EDC/NHS reactions. (B) CV curves of the electrografting process to introduce the −NH$_2$ group on the graphene. (C) Raman spectrum of the graphene surface after electrografting with the −NH$_2$ group. (D) AFM image of graphene surface electrografted with the −NH$_2$ group. (E) Transfer curves of bare G-FET, cleaned G-FET, and G-FET after electrografting (−NH$_2$ group) and dopamine aptamer functionalization. $V_{ds} = 200$ mV. (F) Real-time current response of the dopamine sensor upon exposure to 1× PBS solution containing dopamine with different concentrations: 1 nM, 10 nM, 100 nM, 1 μM, 10 μM, and 100 μM. The current response is defined as $\Delta I_{ds}/I_0 \times 100\%$, where ΔI_{ds} and I_0 are the change of the source−drain current in the presence of the target and the initial current signal without the target, respectively. $V_{ds} = 100$ mV; $V_G = 0$ mV. (G) Selectivity of dopamine sensor. 5-HT: serotonin; DA: dopamine; NE: norepinephrine; GABA: γ-aminobutyric acid.

detection (LOD) of as low as 10 pM. To investigate the molecular specificity of the functionalized G-FET serotonin sensor, the electrical response of the serotonin sensor was monitored when exposed to other neurochemicals, which had concentrations three orders of magnitude higher than that of serotonin, including dopamine, norepinephrine, and γ-aminobutyric acid (Figure 2G). Compared to the response when exposed to 100 μM dopamine, norepinephrine and γ-aminobutyric acid, the serotonin sensor showed at least a 17 times higher response when exposed to 100 nM serotonin, indicating its high selectivity for serotonin monitoring.

2.3. Electrografting of the −NH$_2$ Group and Functionalization of the Dopamine Aptamer on G-FET. The −Ph-NH$_2$ group was electrografted on the graphene surface through the diazonium reaction (Figure 3A). Briefly, the selected G-FET pattern was used as a working electrode and then immersed into the prepared diazonium salt (ClN$_2^+$ −Ph-NH$_2$) solution to link the −Ph-NH$_2$ on the graphene surface by using CV scans for five cycles from −0.6 to 0.5 V (scan rate = 100 mV s^{-1}). After the first cycle, the reduction peak at −0.2 V disappeared, while stable CV curves formed after the second cycle, indicating the electrochemical reduction of ClN$_2^+$-Ph-NH$_2$ to −Ph-NH$_2$ on the graphene surface (Figure 3B). From the Raman spectrum (Figure 3C), we observed a high intensity of the D band and an I_{2D}/I_G ratio of 1.32, indicating a covalent functionalization of the graphene surface after the electrografting. AFM images demonstrated the

formation of rough structures on the graphene surface after the electrografting process, which provides additional evidence to show the success of the diazonium reaction (Figure 3D). The electrografting of −NH$_2$ group was further supported by the CV scan of G-FET (electrolyte containing 1 mM Fe(CN)$_6^{3-}$ and 0.10 M KNO$_3$), in which a significantly reduced anodic current was observed after the electrografting process (Figure S3).

The transfer curves of the bare G-FET, cleaned G-FET, and G-FET with electrografting (-NH$_2$ group) and dopamine aptamer functionalization are shown in Figure 3E. A reduction of the source−drain current and p-doping effect were observed after the electrografting process, mainly due to the diazonium reaction, which broke the sp^2 bond of graphene and introduced the −Ph-NH$_2$ group. Like the serotonin aptamer, surface functionalization with the dopamine aptamer caused a left shift of the transfer curves. To study the sensing performance of the G-FET dopamine sensor, G-FETs functionalized with dopamine aptamers were exposed to the target solution with various concentrations. As seen in Figure 3F, the electrical response increases with the increase of physiologically relevant dopamine concentration ranging from 1 nM to 100 μM in 1× PBS. Signal drifts were observed in Figure 3F, which could be attributed to imperfect binding and the resulting rearrangement of aptamer structures and to the non-specific adsorption on the graphene surface. It has been known that FSCV lacks the molecular specificity to distinguish dopamine from

norepinephrine due to the overlap of voltammetric patterns.[45,78] To investigate whether the G-FET dopamine sensors could distinguish dopamine from norepinephrine and other neurochemicals, the electrical response of the dopamine sensor was recorded when exposed to other neurochemicals that had concentrations three orders of magnitude higher than that of dopamine (Figure 3G). Compared to the electrical responses toward the detection of 100 μM norepinephrine, serotonin, and γ-aminobutyric acid solution, the dopamine sensor showed a 22 times higher response toward the detection of 100 nM dopamine, indicating a high molecular specificity of the dopamine sensors.

2.4. Electrografting-Enabled Site-Selective Functionalization of both Serotonin and Dopamine Aptamers on G-FETs for Multiplexed Neurochemical Monitoring. To enable the simultaneous monitoring of dopamine and serotonin in a single neural probe, the graphene surfaces of two G-FETs were sequentially functionalized with −COOH and −NH$_2$ through the electrografting method (Figure 4A). After that, through the EDC/NHS reaction, the serotonin aptamer with the −NH$_2$ group and the dopamine aptamer with the −COOH group were able to selectively link on the graphene surfaces functionalized with −COOH and −NH$_2$, respectively. Figure 4A illustrates the electrografting and functionalization process of G-FETs for multiplexed neural probe design. One of the major challenges for multiplexed detection in a single neural probe is the crosstalk and interferences between the two sensors. Here, to study the possible interferences between the dopamine and serotonin sensors, we simultaneously measured the electrical response of dopamine and serotonin sensors toward the detection of dopamine and serotonin ranging from 10 pM to 100 μM (Figure 4B,C). The response of the serotonin sensor decreased with the increase of serotonin concentration ranging from 10 pM to 100 μM in 1× PBS. In contrast, the response of the dopamine sensor only slightly increased (∼1.1%) toward the detection of interfering serotonin with a concentration of up to 100 μM (Figure 4B and Table S1). Figure 4C shows the real-time response of dopamine and serotonin sensors when exposing the multiplexed neural probe to various dopamine concentrations ranging from 10 pM to 100 μM in 1× PBS. Like serotonin sensors, the dopamine sensors achieve a LOD of 10 pM. A minimal sensor response (∼ −0.6%) was observed when exposing the serotonin sensor to interfering dopamine with a concentration of up to 100 μM (Figure 4C and Table S2). The minimal crosstalk and interference are further highlighted by measuring the transfer characteristics of G-FET serotonin sensors exposed to dopamine and G-FET dopamine sensors exposed to serotonin (Figure S4). Overall, these studies demonstrate the feasibility of multiplexed monitoring of dopamine and serotonin in a single neural probe with small crosstalk and interferences, suggesting its potential to study the corelease of multiple neurochemicals in broad neuroscience applications.

In this study, we observed a decrease in electrical response ($V_G = 0$ mV) with the increase of serotonin concentration mainly due to the conformational change of aptamer in the presence of serotonin bringing the aptamer away from the graphene channel,[58] leading to a decrease of transconductance and an n-doping effect on graphene surface (Figure 4D). Different from the serotonin aptamer, the presence of dopamine causes an increase in the source−drain current of the G-FET dopamine sensor ($V_G = 0$ mV), mainly due to the
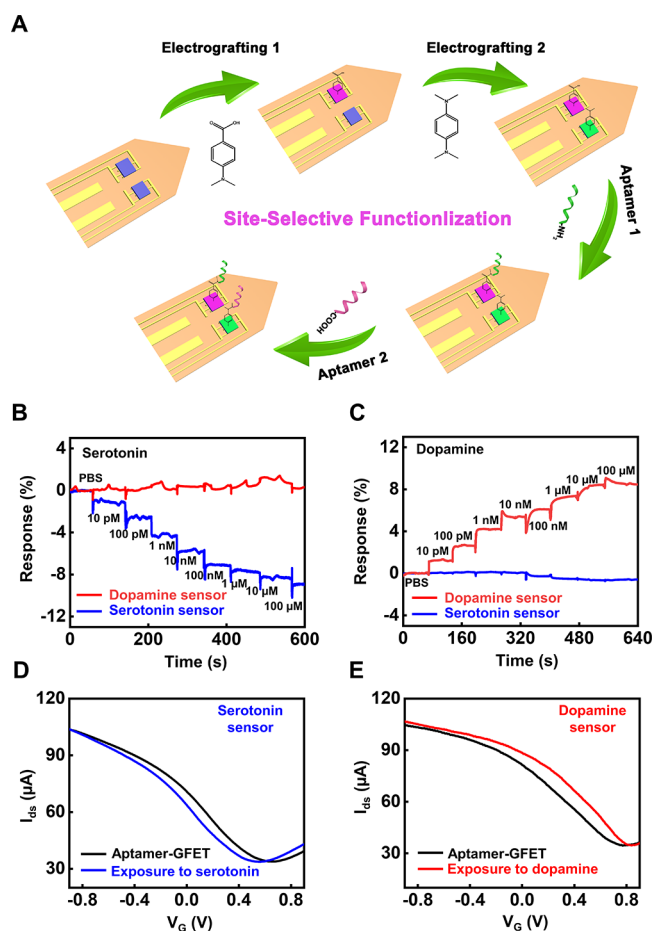

Figure 4. Electrografting-enabled site-selective functionalization of G-FETs for multiplexed neurochemical monitoring in a single neural probe. (A) Schematic illustration for the electrografting and functionalization process of G-FETs for multiplexed monitoring. The graphene surfaces of two G-FETs are sequentially functionalized with −COOH and −NH$_2$ groups through the electrografting method. After that, the serotonin aptamer with the −NH$_2$ group and dopamine aptamer with the −COOH group are immobilized on the graphene surfaces functionalized with −COOH and −NH$_2$, respectively. (B) Real-time response of serotonin and dopamine sensors when exposing a multiplexed neural probe to various serotonin concentrations ranging from 10 pM to 100 μM in 1× PBS. $V_{ds} = 100$ mV; $V_G = 0$ mV. (C) Real-time response of dopamine and serotonin sensors when exposing a multiplexed neural probe to various dopamine concentrations ranging from 10 pM to 100 μM in 1× PBS. $V_{ds} = 100$ mV; $V_G = 0$ mV. (D) Transfer curves of the G-FET serotonin sensor before and after introducing the target serotonin solution (100 μM in 1× PBS). $V_{ds} = 200$ mV. (E) Transfer curves of G-FET dopamine sensor before and after introducing the target dopamine solution (100 μM in 1× PBS). $V_{ds} = 200$ mV.

conformation change of dopamine aptamer, bringing it closer to the G-FET surface,[58] leading to a p-doping effect on G-FET (Figure 4E).

2.5. Multiplexed Monitoring in aCSF with BSA. To evaluate the sensing performance of aptamer-functionalized multiplexed neural probes in a more complex environment, we exposed the dopamine and serotonin sensors to solutions with various concentrations of dopamine or serotonin in aCSF with proteins [1 mg/mL bovine serum albumin (BSA), 13 mM glucose, 125 mM NaCl, 3 mM KCl, 2.5 mM CaCl$_2$, 1.3 mM MgSO$_4$, 1.25 mM NaH$_2$PO$_4$, and 26 mM NaHCO$_3$]. BSA, as a

commonly used protein, was chosen to mimic the protein-rich brain microenvironment.[79] As shown in Figure 5A,B, the
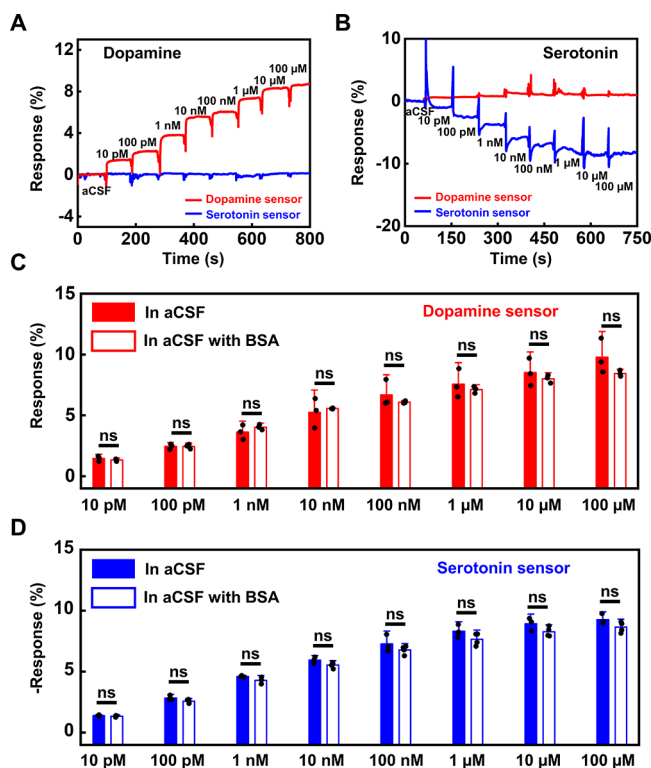
Figure 5. Multiplexed neurochemical monitoring in aCSF with BSA protein. Real-time response of the multiplexed neural probes when exposed to various concentrations of (A) dopamine and (B) serotonin solutions ranging from 10 pM to 100 μM in aCSF with 1 mg/mL BSA protein. V_{ds} = 100 mV; V_G = 0 mV. Comparison of the electrical response of the multiplexed neural probes for monitoring (C) dopamine and (D) serotonin detection with and without 1 mg/mL BSA protein. $n \geq 3$. All data are represented as means ±SD. The statistical significance of differences between mean values was determined using Student's t tests for two independent means with one-tailed hypothesis. ns indicates that the difference of the means is not significant at the 0.05 level.

electrical response increases/decreases with the increase of the physiologically relevant concentration range of dopamine or serotonin from 10 pM to 100 μM. In addition, no significant differences were observed in the sensor response with the addition of 1 mg/mL BSA in aCSF (Figure 5C,D), demonstrating the potential applications of multiplexed neural probes in protein-rich brain microenvironments.

2.6. The Stability of Multiplexed Neural Probes in Rat CSF. Furthermore, we studied the stability of aptamer-functionalized G-FET dopamine and serotonin sensors in rat CSF (BioIVT Elevating Science). The study started with monitoring the transfer curve of aptamer-functionalized G-FETs before and after incubating in rat CSF at room temperature for 24, 48, 72, and 96 h. It is not surprising that a significant leftward downshift of transfer curves are observed after incubating the device in rat CSF for 24 h (Figure 6A and Figure S5), probably due to the non-specific adsorption of proteins in rat CSF on the sensor surface. We then wondered whether this leftward downshift of transfer curves influenced the capability of multiplexed neural probes to monitor dopamine and serotonin. To answer this question, after
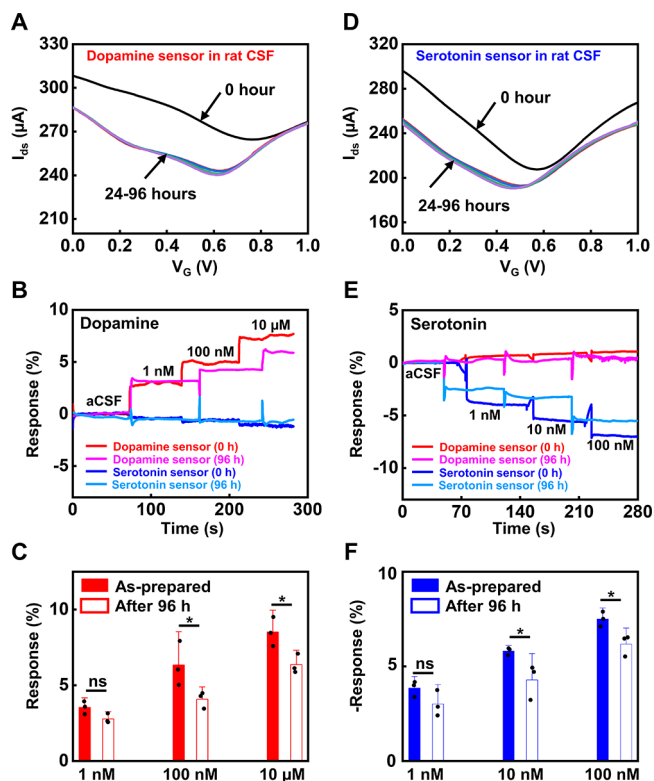
Figure 6. Stability of multiplexed neural probes in rat CSF. (A) Transfer curves of dopamine sensors before and after incubating in rat CSF for 24, 48, 72, and 96 h at room temperature. V_{ds} = 200 mV. (B) Real-time responses of the multiplexed neural probes to various concentrations of dopamine in aCSF before and after incubating in rat CSF solution for 96 h at room temperature. V_{ds} = 100 mV; V_G = 0 mV. (C) Comparison of the sensor response for monitoring dopamine before and after incubating in rat CSF solution at room temperature for 96 h. (D) Transfer curves of serotonin sensors before and after incubating in rat CSF for 24, 48, 72, and 96 h at room temperature. V_{ds} = 200 mV. (E) Real-time responses of the multiplexed neural probes to various concentrations of serotonin in aCSF before and after incubating in rat CSF solution for 96 h at room temperature. V_{ds} = 100 mV; V_G = 0 mV. (F) Comparison of the sensor response for monitoring serotonin before and after incubating in rat CSF solution for 96 h at room temperature. For C and F, n = 3, *P < 0.05. All data are represented as means ±SD. The statistical significance of differences between mean values was determined using Student's t tests for two independent means with one-tailed hypothesis. ns indicates that the difference of the means is not significant at the 0.05 level.

incubating in rat CSF at room temperature for 96 h, we used multiplexed neural probes to monitor different concentrations of dopamine ranging from 1 nM to 10 μM in aCSF. As shown in Figure 6B, the electrical responses of dopamine sensors increase with the increase of the physiologically relevant concentration range of dopamine from 1 nM to 10 μM. In contrast, a minimal sensor response was observed for serotonin sensors (Figure 6B). Compared with the electrical responses of the as-prepared multiplexed neural probes, the incubation with rat CSF for 96 h causes a reduction of sensor signals at higher concentrations (100 nM and 10 μM) (Figure 6C), probably due to the non-specific adsorption of various proteins in the complex rat CSF on the sensor surface that could block the available aptamers to capture the dopamine. Inspired by these stability studies of monitoring dopamine, we also studied the stability of multiplexed neural probes for

monitoring serotonin by incubating the probe in rat CSF at room temperature for 24, 48, 72, and 96 h (Figure 6D−F). Like dopamine sensors, we observed a leftward downshift of transfer curves (Figure 6D) as well as a reduction of sensor response for monitoring higher concentrations of serotonin (10 nM and 100 nM) (Figure 6F). Nevertheless, the multiplexed neural probe retained the capability of monitoring serotonin ranging from 1 to 100 nM in aCSF with minimal crosstalk (Figure 6E). Overall, these studies showed that multiplexed neural probes maintain the ability to simultaneously monitor dopamine and serotonin with minimal crosstalk after incubating in rat CSF at room temperature for 96 h, although a reduced sensor response was observed at a higher concentration range, likely due to the adsorption of proteins onto the sensor surface.

2.7. Ex Vivo Studies in Harvested Mice Brain Tissue.
Encouraged by the capability of multiplexed neural probes for simultaneously monitoring dopamine and serotonin after incubating in rat CSF, we finally evaluated the sensing performance of aptamer-functionalized G-FET dopamine and serotonin sensors in ex vivo brain tissues harvested from wild-type C57BL/6J mice. Figure 7A,B shows the schematic illustration and optical image of the measurement setup where a multiplexed neural probe is implanted into the mouse's brain tissue and an Ag/AgCl electrode is used as a gate. It should be noted that bioresorbable or removable implantation shuttles are typically used for the precise implantation of soft neural probes into targeted brain regions.[80] For those ex vivo studies in harvested mice brain tissues, we do not have a concern about brain damage and associated immune responses. Therefore, we fabricated aptamer−gFET sensors on a relatively thick PI substrate (76 μm thick) to avoid the need for implantation shuttles or tungsten stiffeners for precise probe implantation.

To mimic the evoked release and diffusion of dopamine and serotonin in brain tissue by using electrical and/or pharmacological stimulations, the dopamine (10 μM, 2 μL) or serotonin solution (100 nM, 2 μL) was infused into the brain tissue through the injection site by using a Hamilton microsyringe. These concentrations were chosen to represent a physiologically relevant dopamine[81] or serotonin[36] release upon pharmacology and/or electrical stimulations. The electrical response of dopamine and serotonin sensors rapidly changes upon the injection and diffusion of dopamine or serotonin solution into the brain tissue and then slowly decays due to dopamine or serotonin diffusing away from the sensor surface (Figure 7C,D). To further prove the capability of aptamer-functionalized G-FET dopamine and serotonin sensors to record diffusion-related changes in dopamine or serotonin concentration in harvested brain tissue, we performed real-time monitoring of the transfer curves (instead of the source−drain current) upon the injection of dopamine or serotonin solution in harvested mouse's brain tissue (Figure 7E,F). We observed that the transfer curves of dopamine sensors first shifted to the right and then to the left due to the p-doping effect on G-FET upon the conformation change of dopamine aptamer in the presence of target dopamine (Figure 7E). In contrast, the transfer curves of serotonin sensors first shifted to the left and then to the right because the conformal changes of serotonin aptamer resulted in an n-doping effect on G-FET (Figure 7F). With a fixed-gate voltage (V_G) of 0 mV, the change of source−drain current (I_{ds}) rapidly increases/ decreases and then slowly decays with the injection of
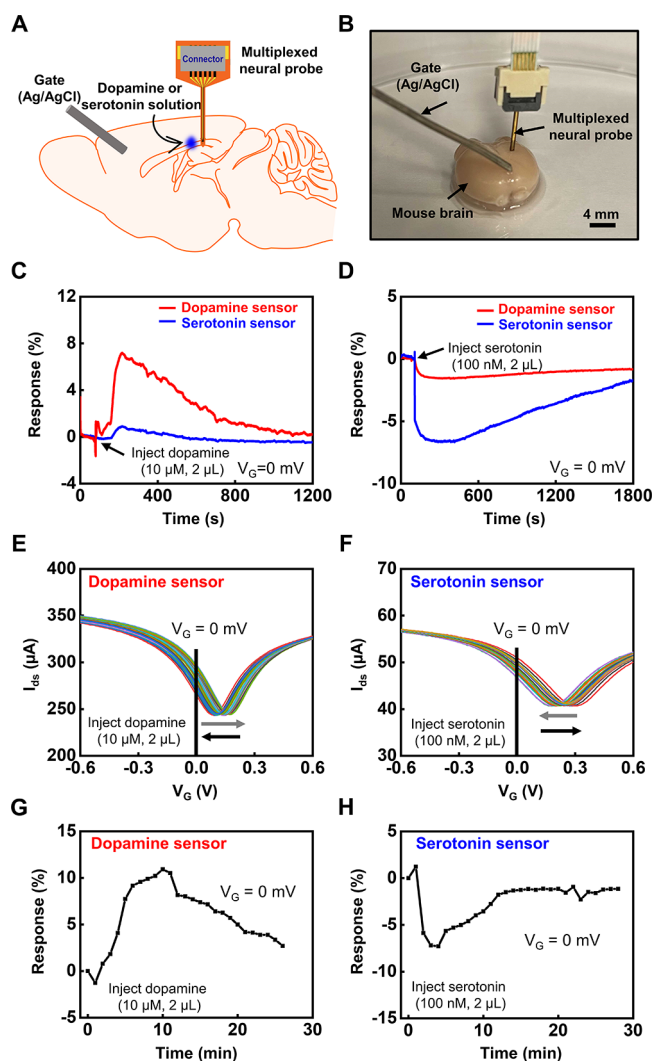
Figure 7. Ex vivo studies in harvested mouse brain tissue. (A) Schematic illustration and (B) optical image of a multiplexed neural probe implanted into a harvested mouse brain tissue for monitoring dopamine and serotonin. Real-time response of a multiplexed neural probe implanted in the harvested mouse brain tissue upon the injection of (C) dopamine solution (10 μM in aCSF, 2 μL) and (D) serotonin solution (100 nM in aCSF, 2 μL). V_{ds} = 100 mV; V_G = 0 mV. Continuous monitoring of transfer curves of the neural probe implanted in the harvested mouse brain tissue when injecting (E) dopamine solution (10 μM in aCSF, 2 μL) and (F) serotonin solution (100 nM in aCSF, 2 μL). V_{ds} = 200 mV. Source−drain current response at V_G = 0 mV for the (G) dopamine and (H) serotonin sensors.

dopamine or serotonin solution (Figure 7G,H), which is consistent with the real-time source−drain current monitoring. In our control experiments, the sensor signal changes induced by injecting 2 μL of aCSF are much smaller than those caused by the perfusion of 2 μL of 100 nM serotonin or 10 μM dopamine in aCSF (Figures S6 and S7). To further mimic the evoked release and diffusion of dopamine or serotonin, the continuous transfer curve monitoring was also performed in brain tissue phantom (0.6 wt % agarose in 1× PBS and soaked in 1× PBS for 24 h) upon the infusion of dopamine or serotonin solution (Figure S8A). Like the study in harvested brain tissues, the transfer curves of dopamine sensors shift to the right first and then to the left (Figure S8B), while the

transfer curves of serotonin sensors shift to the left first and then to the right (Figure S8C). The source−drain current at the fixed-gate voltage of 0 mV increases (or decreases) first and then shows a slow decay (Figures S8D,E), mainly due to the binding between the aptamer and the target (rapidly increase or decrease) upon the injection of target solution and the diffusion of the target molecules away from the sensor surface (slow decay). Overall, these ex vivo studies in harvested mice brain tissue and studies in brain tissue phantom suggest the potential application of aptamer-functionalized multiplexed neural probes for monitoring the evoked release of dopamine and serotonin in vivo.

3. CONCLUSIONS

In summary, we developed a soft neural probe for the multiplexed monitoring of dopamine and serotonin, two important neurochemicals playing critical roles in mood control, rewarding, motor control, and reinforcement learning. The multiplexed neural probes are developed based on the electrochemically grafted site-selective functionalization of −COOH and −NH$_2$ onto an ultrasensitive G-FET and sequential surface functionalization with targeted aptamers. The developed multiplexed neural probes show high sensitivity, molecular specificity, nearly cellular-scale spatial resolution, and minimal crosstalk. The neural probes maintain the ability to perform multiplexed monitoring of dopamine and serotonin after incubating in rat CSF for 96 h at room temperature. Ex vivo studies using harvested mouse brain tissue demonstrate the multiplexed monitoring of dopamine and serotonin upon injecting physiologically relevant concentrations of dopamine or serotonin solutions. Future work is needed to develop surface coatings to prevent protein adsorption on the sensor surface and study the corelease of dopamine and serotonin through in vivo studies. Overall, this study opens the door for neuroscientists to study where and how the corelease of multiple neurochemicals modulates the diverse outputs of the brain. The developed multiplexed neural probes can also be adapted to interface with other organs, including the spinal cord, heart, and peripheral nerves, where multiplexed detection is needed.

4. EXPERIMENTAL SECTION

4.1. Materials. Chemical vapor deposition (CVD)-grown monolayer graphene was purchased from Graphenea. Polymethyl methacrylate (PMMA, inherent viscosity ≈ 1.25 dL/g (lit.), crystalline), acetone (laboratory reagent, ≥99.5%), anisole (anisole, anhydrous, 99.7%), acetonitrile (ACN, anhydrous, ≥99.8%), hydrochloric acid (HCl, ACS reagent, 37%), tetrabutylammonium hexafluorophosphate (TBAPF$_6$, ACS reagent, ≥98%), sodium nitrite (NaNO$_2$ ACS regent, ≥97%), 4-aminobenzoic acid (p-ABA, ACS reagent, ≥99%), p-phenylenediamine (PPD, 98% (GC)), dimethylaminopropyl)-N-ethylcarbodiimide hydrochloride (EDC), N-hydroxysulfo-succinimide sodium salt (NHS), bovine serum albumin (BSA), agarose, dopamine (DA), serotonin, norepinephrine (NE), and γ-aminobutyric acid (GABA) were purchased from Sigma-Aldrich. Polydimethylsiloxane (PDMS, Sylgard 184) was purchased from Dow SYLGARD. Rat CSF (RAT01CSF-0104036, gender-pooled) was purchased from BioIVT Elevating Science. AZ 5214E, SU8 photoresists were purchased from Integrated Micro Materials. Serotonin aptamer (5′-AmC6-CGA CTG GTA GGC AGA TAG GGG AAG CTG

ATT CGA TGC GTG GGT CG-3′) and dopamine aptamer (5′/COOH/CGA CGC CAG TTT GAA GGT TCG TTC GCA GGT GTG GAG TGA CGT CG) were reported by a previous study[58] and purchased from Integrated DNA Technologies, Inc. All of the chemicals and materials were used without further purification after purchase.

4.2. Fabrication and Electrochemical Cleaning of G-FETs. *4.2.1. Preparation of Graphene Patterns.* A piece of CVD-grown monolayer graphene (Graphenea) was first coated with PMMA A4 solution (4 g of PMMA dissolved in 96 g of anisole) to get the PMMA/graphene/Cu stack, which was then heated at 180 °C for 5 min and slowly cooled down to room temperature. The PMMA/graphene/Cu was further cut into small pieces and floated on the surface of the copper etchant for 5 min to remove the Cu film. After that, the obtained PMMA/graphene film was transferred into 0.1 M HCl for 10 min and then washed with deionized (DI) water three times. A piece of Si wafer was then used to pick up the transferred PMMA/graphene film. After drying in air overnight at room temperature, PMMA A2 solution (2 g of PMMA in 98 g of anisole) was applied onto the surface of the PMMA/graphene/Si to release the possible wrinkles in graphene. Then, PMMA/graphene/Si was immersed into acetone for 4 h to remove the PMMA. The obtained graphene/Si was spin-coated (at 500 rpm for 10 s followed with 1500 rpm for 25 s; acceleration of 300 rmp/s) with the photoresist (AZ5214), followed by baking at 95 °C for 3 min on a hot plate. A predesigned mask was used to form desired patterns on the graphene surface by oxygen plasma. Finally, the graphene pattern with a size of 60 μm × 60 μm was obtained by removing the photoresist with acetone.

4.2.2. Preparation of the Source−Drain Electrodes. A mixture of PDMS elastomer and curing reagent (10:1 ratio) was first spin-coated on a glass slide (75 mm × 50 mm), which was then cured in a 70 °C oven for 10 min. After that, a PI film was laminated onto the semicured PDMS surface, followed by another 50 min curing at 70 °C. Then, the PI film was spin-coated with a AZ5214 photoresist and baked at 95 °C for 3 min on a hot plate. With exposure to UV light through a designed mask and development, interdigitated patterns were formed on the surface of PI film. An RF sputter (AJA Orion-8) was used to deposit Cr with a 15 nm thickness and Au with a 90 nm thickness on top of the patterned PI film. A lift-off process was carried out to form the source−drain electrodes on the soft PI film.

4.2.3. Graphene Transfer to Source−Drain Electrodes and Device Encapsulation. The obtained graphene patterns were first coated with PMMA A4 solution to form a PMMA/graphene/Si stack, which was then heated at 180 °C for 5 min and naturally cooled down to room temperature. Next, the above stack was immersed in 1 mM NaOH solution until the PMMA/graphene pattern stack detached from the Si wafer surface and floated on the solution. The PMMA/graphene pattern was washed with DI water three times and then transferred on the PI film-containing source and drain contact pads under a microscope. Similarly, after overnight drying in the air, the PMMA A2 solution was dropped on the PI film to release the possible wrinkles on the graphene. After immersing the PI film covered by the PMMA/graphene pattern stack into acetone for 4 h, the PMMA layer can be removed to get the graphene pattern on the preconstructed source and drain contact pads. Finally, the source and drain electrodes were encapsulated with SU8 (2000.5, MicroChem) following the

standard photolithography protocol. The final thickness of the SU8 layer and the active sensing area of graphene are 0.8 μm and 50 μm × 50 μm, respectively.

4.2.4. Electrochemical Cleaning of the G-FETs. The fabricated G-FETs were first cleaned by using an electrochemical method.[65] More specifically, a non-aqueous electrolyte containing acetonitrile (Sigma Aldrich) and 100 mM tetrabutylammonium hexafluorophosphate (TBAPF$_6$, Sigma Aldrich) was used to perform the electrochemical cleaning using an Autolab potentiostat (Autolab PGSTAT128N). The G-FET was used as the working electrode (WE) with a platinum wire as a counter electrode (CE) and Ag/AgCl electrode as a reference electrode (RE). The CV was performed under the potential window from −0.7 to 0 V vs. Ag/AgCl at a scan rate of 0.5 V s^{-1} for 100 cycles. After the electrochemical treatment, the cleaned G-FET was rinsed several times using pure acetonitrile and DI water to remove the residual electrolyte from the graphene surface.

4.3. Surface Functionalization of the G-FETs. *4.3.1. Electrochemical Grafting −COOH Group on the Graphene Surface.* The classic diazonium reaction was used for electrochemical grafting of the −COOH group on the graphene surface of G-FET. First, 10 mL of 2 mM NaNO$_2$ solution drops into 10 mL of 2 mM *p*-aminobenzoic acid (*p*-ABA) solution in 1 M HCl solution in 30 min. The mixed solution was then degassed under nitrogen flow for 5 min and left to react in an ice water bath for another 10 min for the formation of the diazonium salt (ClN$_2$$^+$-Ph-COOH). After that, the G-FET was immersed into the above mixture solution to serve as the working electrode. Saturated Ag/AgCl and Pt electrodes were used as the reference electrode and counter electrode, respectively. A CV scan was used to graft -Ph-COOH onto the graphene surface at a scan rate of 100 mV s^{-1} within a voltage window of −0.6 to 0.5 V. Different scan cycles were performed to optimize the electrochemical grafting process to achieve the fully covered graphene surface with −COOH group. Finally, the −COOH-functionalized G-FET was thoroughly rinsed with acetonitrile and DI water to remove the nonspecifically adsorbed substances.

4.3.2. Electrochemical Grafting of the −NH$_2$ Group on the Graphene Surface. The diazonium reaction was also used for electrochemical grafting of the −NH$_2$ group on the graphene surface of G-FET following a similar protocol as that of −COOH electrografting. Here, 10 mL of the 4 mM NaNO$_2$ solution was first added dropwise into 10 mM phenylenediamine (PPD) in 1 M HCl solution. After degassing using nitrogen flow for 5 min, the mixed solution was left in an ice water bath for 10 min to form diazonium salt (ClN^{2+}-Ph-NH$_2$). CV scans were performed at a scan of 100 mV s^{-1} in the potential window of −0.6 to 0.5 V for five cycles to graft the −NH$_2$ group on the graphene surfaces of G-FET. Finally, the obtained −NH$_2$-grafted G-FET was thoroughly rinsed with acetonitrile and ultrapure DI water to remove the nonspecifically adsorbed substances.

4.3.3. Surface Functionalization of the Aptamers through EDC/NHS Reactions. For the functionalization of G-FETs with serotonin aptamers, the electrografted G-FETs with −COOH groups were incubated in 1× PBS solution containing 6 mM EDC, 3 mM NHS, and 3 μM amino group-modified serotonin aptamer (5′-AmC6-CGA CTG GTA GGC AGA TAG GGG AAG CTG ATT CGA TGC GTG GGT CG-3′) at room temperature for 4 h. After that, the functionalized G-FETs

linked with serotonin aptamers were washed with DI water and dried with N$_2$ gas.

For the functionalization of G-FETs with dopamine aptamers, the electrografted G-FETs with −NH$_2$ groups were first incubated in the 1× PBS solution containing 6 mM EDC, 3 mM NHS, and 3 μM carboxyl group-modified dopamine aptamer (5′/COOH/CGA CGC CAG TTT GAA GGT TCG TTC GCA GGT GTG GAG TGA CGT CG,) at room temperature for 4 h. After that, the functionalized G-FETs linked with dopamine aptamers were washed with DI water and dried with N$_2$ gas.

4.4. Materials Characterization and Sensing Performance Evaluation. *4.4.1. Materials Characterization.* The pattern and graphene microstructure of the prepared G-FETs were characterized by scanning electron microscopy (SEM; Teneo LV SEM equipped with energy-dispersive X-ray spectroscopy (EDS) detector), atomic force microscopy (AFM; mfp-3D operating in conventional intermittent contact, Asylum Research), and Raman spectroscopy (Renishaw InVia Raman microscope at 575 nm with 10% laser power). Electrical measurement was performed with the Keysight B1500A Semiconductor Analyzer and probe station.

4.4.2. Sensing Performance Evaluation. 4.4.2.1. Real-Time Response of the Functionalized G-FETs. The real-time response of the functionalized G-FETs with serotonin aptamers was performed using the Keysight B1500A Semiconductor Analyzer and probe station. Each time, 20 μL of the test solution was put on the sensing area of the G-FET to record the response. After that, the test solution was quickly removed using Kimwipes, and the next test solution was added immediately using a second pipette. A series of freshly prepared serotonin solutions were used to evaluate the sensing performance of the fabricated G-FETs with serotonin aptamers. Similarly, the real-time response of G-FETs with dopamine aptamers was evaluated by gradually adding freshly prepared dopamine solution.

4.4.2.2. Selectivity of the Functionalized G-FETs Sensor. The selectivity of the functionalized G-FETs with dopamine or serotonin aptamers was evaluated by recording the electrical response when the G-FETs were exposed to different neurotransmitters, such as dopamine, serotonin, norepinephrine, and γ-aminobutyric acid.

4.5. Tissue Collection. Adult C57BL/6J mice obtained from Jackson Laboratories were used for all experiments. Mice were first anesthetized with 5% isoflurane in an induction chamber and then held under anesthesia with a nose cone throughout the procedure. An incision was made along the ventral surface of the mouse to expose the diaphragm, which was then separated from the rib cage. The rib cage was excised to expose the heart. Using a pair of blunt forceps, the heart was stabilized, and a needle for perfusion was inserted into the left ventricle. A small incision was then made in the right atrium of the heart, and 15 mL of aCSF was perfused through the animal. Once perfused, the mice were decapitated, and the dorsal surface of the skull was exposed with a midline incision through the skin. The skull is then opened to expose the brain, which is subsequently extracted and placed in aCSF. All experiments performed were approved by the University of Connecticut Institutional Animal Care and Use Committee Institutional Animal Care and Use Committee (IACUC).

4.6. Statistics. Experimental data are expressed as the mean ± standard deviation (SD). For two-group comparisons, statistical significance was determined by one-tailed Student's *t*

tests. $P < 0.05$ was considered statistically significant. The software used for statistical analysis was OriginLab.

ASSOCIATED CONTENT

Supporting Information

The Supporting Information is available free of charge at https://pubs.acs.org/doi/10.1021/acs.analchem.1c05531.

(Figure S1) Schematic illustration of the preparation of contact pads (source−drain) on the polyimide (PI) substrate and transferring graphene to the contact pads; (Figures S2 and S3) CV curves of G-FET before and after the electrografting with a carboxyl group and an amino group; (Figure S4) transfer characteristics of a G-FET serotonin sensor exposed to dopamine and dopamine sensor exposed to serotonin;(Figure S5) change of the voltage at Dirac point (V_{dp}) of dopamine and serotonin sensors after incubating in rat CSF solution at room temperature for 24, 48, 72, and 96 h; (Figure S6) ex vivo studies of dopamine sensors in harvested mouse's brain tissue; (Figure S7) ex vivo studies of serotonin sensors in harvested mouse's brain tissue; (Figure S8) in vitro studies using brain tissue phantom models; (Table S1) responses of serotonin and dopamine sensors when exposing a multiplex neural probe into various serotonin concentrations; (Table S2) responses of dopamine and serotonin sensors when exposing a multiplex neural probe to various dopamine concentrations (PDF)

AUTHOR INFORMATION

Corresponding Author

Yi Zhang − *Department of Biomedical Engineering and the Institute of Materials Science, University of Connecticut, Storrs, Connecticut 06269, United States;* ⊙ orcid.org/0000-0002-0907-663X; Email: yi.5.zhang@uconn.edu

Authors

Zan Gao − *Department of Biomedical Engineering and the Institute of Materials Science, University of Connecticut, Storrs, Connecticut 06269, United States*

Guangfu Wu − *Department of Biomedical Engineering and the Institute of Materials Science, University of Connecticut, Storrs, Connecticut 06269, United States*

Yang Song − *Department of Biomedical Engineering and the Institute of Materials Science, University of Connecticut, Storrs, Connecticut 06269, United States;* ⊙ orcid.org/0000-0003-0626-0850

Huijie Li − *Department of Biomedical Engineering and the Institute of Materials Science, University of Connecticut, Storrs, Connecticut 06269, United States*

Yuxuan Zhang − *Department of Biomedical Engineering and the Institute of Materials Science, University of Connecticut, Storrs, Connecticut 06269, United States*

Michael J. Schneider − *Department of Biomedical Engineering and the Institute of Materials Science, University of Connecticut, Storrs, Connecticut 06269, United States;* ⊙ orcid.org/0000-0003-1435-1584

Yingqi Qiang − *Department of Biomedical Engineering and the Institute of Materials Science, University of Connecticut, Storrs, Connecticut 06269, United States;* ⊙ orcid.org/0000-0001-8763-2323

Jackson Kaszas − *Department of Materials Science and Engineering and the Institute of Materials Science, University of Connecticut, Storrs, Connecticut 06269, United States*

Zhengyan Weng − *Department of Biomedical Engineering and the Institute of Materials Science, University of Connecticut, Storrs, Connecticut 06269, United States*

He Sun − *Department of Biomedical Engineering and the Institute of Materials Science, University of Connecticut, Storrs, Connecticut 06269, United States*

Bryan D. Huey − *Department of Materials Science and Engineering and the Institute of Materials Science, University of Connecticut, Storrs, Connecticut 06269, United States*

Rebecca Y. Lai − *Department of Chemistry, University of Nebraska-Lincoln, Lincoln, Nebraska 68588, United States;* ⊙ orcid.org/0000-0002-1732-9481

Complete contact information is available at:
https://pubs.acs.org/10.1021/acs.analchem.1c05531

Author Contributions

‖Z.G., G.W., Y.S. contributed equally to this work.

Author Contributions

Z.G., G.W., and Y.Z. conceived the idea and designed the experiments; G.W., H.L., and Y.Q. designed and fabricated graphene field-effect transistors; Z.G., Y.S., Y.Z., Z.W., and H.S. contributed to the electrografting, functionalization, and characterizations. J.K. and B.D.H. performed the AFM measurements. M.S. collected the mouse brain tissue for ex vivo studies. R.L. provided guidance regarding the site-selective functionalization via electrografting. Z.G., G.W., Y.S., and Y.Z. analyzed the data and wrote the manuscript. All authors discussed the results and contributed to the final manuscript.

Notes

The authors declare no competing financial interest.

ACKNOWLEDGMENTS

REFERENCES

(1) Myhrer, T. *Brain Res. Rev.* **2003**, *41*, 268−287.
(2) Wise, R. A. *Nat. Rev. Neurosci.* **2004**, *5*, 483−494.
(3) Webster, R., *Neurotransmitters, drugs and brain function*. John Wiley & Sons: 2001.
(4) Ngernsutivorakul, T.; White, T. S.; Kennedy, R. T. *ChemPhysChem* **2018**, *19*, 1128−1142.
(5) Jankovic, J. *Brain* **2018**, *141*, 624−626.
(6) Joling, M.; van den Heuvel, O. A.; Berendse, H. W.; Booij, J.; Vriend, C. *J. Neurol., Neurosurg. Psychiatry* **2018**, *89*, 89−94.
(7) Sitte, H. H.; Pifl, C.; Rajput, A. H.; Hortnagl, H.; Tong, J.; Lloyd, G. K.; Kish, S. J.; Hornykiewicz, O. *Eur. J. Neurosci.* **2017**, *45*, 1356.
(8) Pagano, G.; Niccolini, F.; Fusar-Poli, P.; Politis, M. *Ann Neurol* **2017**, *81*, 171−180.
(9) Stahl, S. M. *CNS Spectr* **2016**, *21*, 355−359.
(10) Blum, R.; Lesch, K. P. *J. Neurochem.* **2015**, *135*, 441−444.
(11) McCutcheon, R. A.; Abi-Dargham, A.; Howes, O. D. *Trends Neurosci.* **2019**, *42*, 205−220.
(12) Francis, P. T. *Int. J. Geriatr. Psychiatry* **2003**, *18*, S15−S21.
(13) Saunders, A.; Granger, A. J.; Sabatini, B. L. *Elife* **2015**, *4*, No. e06412.
(14) Root, D. H.; Mejias-Aponte, C. A.; Zhang, S.; Wang, H. L.; Hoffman, A. F.; Lupica, C. R.; Morales, M. *Nat. Neurosci.* **2014**, *17*, 1543−1551.

(15) Shabel, S. J.; Proulx, C. D.; Piriz, J.; Malinow, R. *Science* **2014**, *345*, 1494−1498.

(16) Barker, D. J.; Root, D. H.; Zhang, S.; Morales, M. *J. Chem. Neuroanat.* **2016**, *73*, 33−42.

(17) Yoo, J. H.; Zell, V.; Gutierrez-Reed, N.; Wu, J.; Ressler, R.; Shenasa, M. A.; Johnson, A. B.; Fife, K. H.; Faget, L.; Hnasko, T. S. *Nat Commun.* **2016**, *7*, 13697.

(18) Zhou, F. M.; Liang, Y.; Salas, R.; Zhang, L.; De Biasi, M.; Dani, J. A. *Neuron* **2005**, *46*, 65−74.

(19) Eskenazi, D.; Malave, L.; Mingote, S.; Yetnikoff, L.; Ztaou, S.; Velicu, V.; Rayport, S.; Chuhma, N. *Front. Neural Circuits.* **2021**, *15*, 665386.

(20) Patriarchi, T.; Cho, J. R.; Merten, K.; Howe, M. W.; Marley, A.; Xiong, W. H.; Folk, R. W.; Broussard, G. J.; Liang, R.; Jang, M. J.; Zhong, H.; Dombeck, D.; von Zastrow, M.; Nimmerjahn, A.; Gradinaru, V.; Williams, J. T.; Tian, L. *Science* **2018**, *360*, eaat4422.

(21) Xu, C.; Wu, F.; Yu, P.; Mao, L. *ACS Sens.* **2019**, *4*, 3102−3118.

(22) Tan, C.; Robbins, E. M.; Wu, B.; Cui, X. T. *Micromachines* **2021**, *12*, 208.

(23) Drevets, W. C.; Price, J. C.; Kupfer, D. J.; Kinahan, P. E.; Lopresti, B.; Holt, D.; Mathis, C. *Neuropsychopharmacology* **1999**, *21*, 694−709.

(24) Moody, A. S.; Sharma, B. *ACS Chem. Neurosci.* **2018**, *9*, 1380−1387.

(25) Bell, S. E.; Park, I.; Rubakhin, S. S.; Bashir, R.; Vlasov, Y.; Sweedler, J. V. *ACS Measurement Science Au* **2021**, *1*, 147−156.

(26) Leopold, A. V.; Shcherbakova, D. M.; Verkhusha, V. V. *Front Cell Neurosci* **2019**, *13*, 474.

(27) Liang, R.; Broussard, G. J.; Tian, L. *ACS Chem. Neurosci.* **2015**, *6*, 84−93.

(28) Nalewajko, E.; Bort Ramirez, R.; Kojlo, A. *J. Pharm. Biomed. Anal.* **2004**, *36*, 219−223.

(29) Zibaii, M.; Latifi, H.; Asadollahi, A.; Bayat, A. H.; Dargahi, L.; Haghparast, A. *J. Lightwave Technol.* **2016**, *34*, 4516−4524.

(30) Lin, Y.; Chen, C.; Wang, C.; Pu, F.; Ren, J.; Qu, X. *Chem. Commun.* **2011**, *47*, 1181−1183.

(31) Xiao, T.; Wu, F.; Hao, J.; Zhang, M.; Yu, P.; Mao, L. *Anal. Chem.* **2017**, *89*, 300−313.

(32) Xue, Y.; Ji, W.; Jiang, Y.; Yu, P.; Mao, L. *Angew. Chem.* **2021**, *60*, 23777−23783.

(33) Abdalla, A.; Atcherley, C. W.; Pathirathna, P.; Samaranayake, S.; Qiang, B.; Pena, E.; Morgan, S. L.; Heien, M. L.; Hashemi, P. *Anal. Chem.* **2017**, *89*, 9703−9711.

(34) Venton, B. J.; Cao, Q. *Analyst* **2020**, *145*, 1158−1168.

(35) Castagnola, E.; Garg, R.; Rastogi, S. K.; Cohen-Karni, T.; Cui, X. T. *Biosens. Bioelectron.* **2021**, *191*, No. 113440.

(36) Shin, H.; Oh, Y.; Park, C.; Kang, Y.; Cho, H. U.; Blaha, C. D.; Bennet, K. E.; Heien, M. L.; Kim, I. Y.; Lee, K. H.; Jang, D. P. *Anal. Chem.* **2020**, *92*, 774−781.

(37) Westerink, R. H. *Neurotoxicology* **2004**, *25*, 461−470.

(38) Zhao, X. E.; Suo, Y. R. *Talanta* **2008**, *76*, 690−697.

(39) Neumann, E. K.; Comi, T. J.; Spegazzini, N.; Mitchell, J. W.; Rubakhin, S. S.; Gillette, M. U.; Bhargava, R.; Sweedler, J. V. *Anal. Chem.* **2018**, *90*, 11572−11580.

(40) Zestos, A. G.; Kennedy, R. T. *AAPS J* **2017**, *19*, 1284−1293.

(41) Lee, W. H.; Slaney, T. R.; Hower, R. W.; Kennedy, R. T. *Anal. Chem.* **2013**, *85*, 3828−3831.

(42) Zhou, Y.; Wong, J. M.; Mabrouk, O. S.; Kennedy, R. T. *Anal. Chem.* **2015**, *87*, 9802−9809.

(43) Al-Hasani, R.; Wong, J. T.; Mabrouk, O. S.; McCall, J. G.; Schmitz, G. P.; Porter-Stransky, K. A.; Aragona, B. J.; Kennedy, R. T.; Bruchas, M. R. *Elife* **2018**, *7*, No. e36520.

(44) Wu, G.; Heck, I.; Zhang, N.; Phaup, G.; Zhang, X.; Wu, Y.; Stalla, D. E.; Weng, Z.; Sun, H.; Li, H.; Zhang, Z.; Ding, S.; Li, D. P.; Zhang, Y. *Sci. Adv.* **2022**, *8*, eabn2277.

(45) Pradhan, T.; Jung, H. S.; Jang, J. H.; Kim, T. W.; Kang, C.; Kim, J. S. *Chem. Soc. Rev.* **2014**, *43*, 4684−4713.

(46) Zhang, Y.; Jiang, N.; Yetisen, A. K. *Biosens. Bioelectron.* **2021**, *189*, No. 113351.

(47) Wu, Z.; Lin, D.; Li, Y. *Nat Rev Neurosci* **2022**, *23*, 257−274.

(48) Moran, R. J.; Kishida, K. T.; Lohrenz, T.; Saez, I.; Laxton, A. W.; Witcher, M. R.; Tatter, S. B.; Ellis, T. L.; Phillips, P. E.; Dayan, P.; Montague, P. R. *Neuropsychopharmacology* **2018**, *43*, 1425−1435.

(49) Movassaghi, C. S.; Perrotta, K. A.; Yang, H.; Iyer, R.; Cheng, X.; Dagher, M.; Fillol, M. A.; Andrews, A. M. *Anal. Bioanal. Chem.* **2021**, *413*, 6747−6767.

(50) Clark, J. J.; Sandberg, S. G.; Wanat, M. J.; Gan, J. O.; Horne, E. A.; Hart, A. S.; Akers, C. A.; Parker, J. G.; Willuhn, I.; Martinez, V.; Evans, S. B.; Stella, N.; Phillips, P. E. *Nat. Methods* **2010**, *7*, 126−129.

(51) Schwerdt, H. N.; Zhang, E.; Kim, M. J.; Yoshida, T.; Stanwicks, L.; Amemori, S.; Dagdeviren, H. E.; Langer, R.; Cima, M. J.; Graybiel, A. M. *Commun Biol* **2018**, *1*, 144.

(52) Puthongkham, P.; Venton, B. J. *Analyst* **2020**, *145*, 1087−1102.

(53) Chefer, V. I.; Thompson, A. C.; Zapata, A.; Shippenberg, T. S., Overview of brain microdialysis. *Curr. Protoc. Neurosci.* **2009**, *Chapter 7*, Unit7 1.

(54) Anderzhanova, E.; Wotjak, C. T. *Cell Tissue Res.* **2013**, *354*, 27−39.

(55) Sun, F.; Zeng, J.; Jing, M.; Zhou, J.; Feng, J.; Owen, S. F.; Luo, Y.; Li, F.; Wang, H.; Yamaguchi, T.; Yong, Z.; Gao, Y.; Peng, W.; Wang, L.; Zhang, S.; Du, J.; Lin, D.; Xu, M.; Kreitzer, A. C.; Cui, G.; Li, Y. *Cell* **2018**, *174*, 481−496.e19.

(56) Feng, J.; Zhang, C.; Lischinsky, J. E.; Jing, M.; Zhou, J.; Wang, H.; Zhang, Y.; Dong, A.; Wu, Z.; Wu, H.; Chen, W.; Zhang, P.; Zou, J.; Hires, S. A.; Zhu, J. J.; Cui, G.; Lin, D.; Du, J.; Li, Y. *Neuron* **2019**, *102*, 745−761.e8.

(57) Sabatini, B. L.; Tian, L. *Neuron* **2020**, *108*, 17−32.

(58) Nakatsuka, N.; Yang, K. A.; Abendroth, J. M.; Cheung, K. M.; Xu, X.; Yang, H.; Zhao, C.; Zhu, B.; Rim, Y. S.; Yang, Y.; Weiss, P. S.; Stojanovic, M. N.; Andrews, A. M. *Science* **2018**, *362*, 319−324.

(59) Zhao, C.; Cheung, K. M.; Huang, I. W.; Yang, H.; Nakatsuka, N.; Liu, W.; Cao, Y.; Man, T.; Weiss, P. S.; Monbouquette, H. G.; Andrews, A. M. *Sci. Adv.* **2021**, *7*, eabj7422.

(60) Wu, G.; Zhang, N.; Matarasso, A.; Heck, I.; Li, H.; Lu, W.; Phaup, J. G.; Schneider, M. J.; Wu, Y.; Weng, Z.; Sun, H.; Gao, Z.; Zhang, X.; Sandberg, S. G.; Parvin, D.; Seaholm, E.; Islam, S. K.; Wang, X.; Phillips, P. E. M.; Castro, D. C.; Ding, S.; Li, D. P.; Bruchas, M. R.; Zhang, Y. *Nano Lett.* **2022**, *22*, 3668−3677.

(61) Lu, L.; Gutruf, P.; Xia, L.; Bhatti, D. L.; Wang, X.; Vazquez-Guardado, A.; Ning, X.; Shen, X.; Sang, T.; Ma, R.; Pakeltis, G.; Sobczak, G.; Zhang, H.; Seo, D. O.; Xue, M.; Yin, L.; Chanda, D.; Sheng, X.; Bruchas, M. R.; Rogers, J. A. *Proc. Natl. Acad. Sci. U. S. A.* **2018**, *115*, E1374−E1383.

(62) Du, M.; Huang, L.; Zheng, J.; Xi, Y.; Dai, Y.; Zhang, W.; Yan, W.; Tao, G.; Qiu, J.; So, K. F.; Ren, C.; Zhou, S. *Adv. Sci.* **2020**, *7*, 2001410.

(63) Cho, Y.; Park, S.; Lee, J.; Yu, K. J. *Adv. Mater.* **2021**, *33*, No. e2005786.

(64) Luan, L.; Wei, X.; Zhao, Z.; Siegel, J. J.; Potnis, O.; Tuppen, C. A.; Lin, S.; Kazmi, S.; Fowler, R. A.; Holloway, S.; Dunn, A. K.; Chitwood, R. A.; Xie, C. *Sci. Adv.* **2017**, *3*, No. e1601966.

(65) Park, B.; Huh, J. N.; Lee, W. S.; Bae, I.-G. *J. Mater. Chem. C* **2018**, *6*, 2234−2244.

(66) Fu, W.; Jiang, L.; van Geest, E. P.; Lima, L. M.; Schneider, G. F. *Adv. Mater.* **2017**, *29*, 1603610.

(67) Hwang, M. T.; Heiranian, M.; Kim, Y.; You, S.; Leem, J.; Taqieddin, A.; Faramarzi, V.; Jing, Y.; Park, I.; van der Zande, A. M.; Nam, S.; Aluru, N. R.; Bashir, R. *Nat. Commun.* **2020**, *11*, 1543.

(68) Beraud, A.; Sauvage, M.; Bazan, C. M.; Tie, M.; Bencherif, A.; Bouilly, D. *Analyst* **2021**, *146*, 403−428.

(69) Wang, C.; Yan, Q.; Liu, H. B.; Zhou, X. H.; Xiao, S. J. *Langmuir* **2011**, *27*, 12058−12068.

(70) Wickramathilaka, M. P.; Tao, B. Y. *J Biol Eng* **2019**, *13*, 63.

(71) Kesler, V.; Murmann, B.; Soh, H. T. *ACS Nano* **2020**, *14*, 16194−16201.

(72) Gotrik, M. R.; Feagin, T. A.; Csordas, A. T.; Nakamoto, M. A.; Soh, H. T. *Acc. Chem. Res.* **2016**, *49*, 1903−1910.

(73) Rangel, A. E.; Hariri, A. A.; Eisenstein, M.; Soh, H. T. *Adv. Mater.* **2020**, *32*, No. e2003704.

(74) Belanger, D.; Pinson, J. *Chem. Soc. Rev.* **2011**, *40*, 3995−4048.

(75) Eckmann, A.; Felten, A.; Mishchenko, A.; Britnell, L.; Krupke, R.; Novoselov, K. S.; Casiraghi, C. *Nano Lett.* **2012**, *12*, 3925−3930.

(76) Malard, L.; Pimenta, M. A.; Dresselhaus, G.; Dresselhaus, M. *Phys. Rep.* **2009**, *473*, 51−87.

(77) Artigas, F.; Sarrias, M. J.; Martinez, E.; Gelpi, E. *Life Sci.* **1985**, *37*, 441−447.

(78) Roberts, J. G.; Sombers, L. A. *Anal. Chem.* **2018**, *90*, 490−504.

(79) Zhao, F.; Liu, Y.; Dong, H.; Feng, S.; Shi, G.; Lin, L.; Tian, Y. *Angew. Chem.* **2020**, *59*, 10426−10430.

(80) Apollo, N. V.; Murphy, B.; Prezelski, K.; Driscoll, N.; Richardson, A. G.; Lucas, T. H.; Vitale, F. *J. Neural. Eng.* **2020**, *17*, No. 041002.

(81) Ngo, K. T.; Varner, E. L.; Michael, A. C.; Weber, S. G. *ACS Chem. Neurosci.* **2017**, *8*, 329−338.

📖 **Recommended by ACS**

Intradermal Glycine Detection with a Wearable Microneedle Biosensor: The First In Vivo Assay

Qianyu Wang, Maria Cuartero, *et al.*

AUGUST 18, 2022
ANALYTICAL CHEMISTRY

READ 🗗

Aptasensors Based on Graphene Field-Effect Transistors for Arsenite Detection

Jingwei Li, Zhaoli Gao, *et al.*

SEPTEMBER 06, 2022
ACS APPLIED NANO MATERIALS

READ 🗗

Boronate-Affinity Cross-Linking-Based Ratiometric Electrochemical Detection of Glycoconjugates

Qiong Hu, Li Niu, *et al.*

JUNE 21, 2022
ANALYTICAL CHEMISTRY

READ 🗗

Implantable Aptamer-Graphene Microtransistors for Real-Time Monitoring of Neurochemical Release in Vivo

Guangfu Wu, Yi Zhang, *et al.*

APRIL 19, 2022
NANO LETTERS

READ 🗗

Get More Suggestions >